

This article was originally published in a journal published by Elsevier, and the attached copy is provided by Elsevier for the author's benefit and for the benefit of the author's institution, for non-commercial research and educational use including without limitation use in instruction at your institution, sending it to specific colleagues that you know, and providing a copy to your institution's administrator.

All other uses, reproduction and distribution, including without limitation commercial reprints, selling or licensing copies or access, or posting on open internet sites, your personal or institution's website or repository, are prohibited. For exceptions, permission may be sought for such use through Elsevier's permissions site at:

<http://www.elsevier.com/locate/permissionusematerial>



ELSEVIER

Available online at [www.sciencedirect.com](http://www.sciencedirect.com)

 ScienceDirect

Proceedings of the Combustion Institute 31 (2007) 473–481

Proceedings  
of the  
Combustion  
Institute

[www.elsevier.com/locate/proci](http://www.elsevier.com/locate/proci)

# Application of the ICE-PIC method for the dimension reduction of chemical kinetics coupled with transport

Zhuyin Ren <sup>a,\*</sup>, Stephen B. Pope <sup>a</sup>, Alexander Vladimirovsky <sup>b</sup>,  
John M. Guckenheimer <sup>b</sup>

<sup>a</sup> Sibley School of Mechanical and Aerospace Engineering, Cornell University, Ithaca, NY 14853, USA

<sup>b</sup> Department of Mathematics, Cornell University, Ithaca, NY 14853, USA

## Abstract

A new dimension-reduction method, the Invariant Constrained-equilibrium Edge Pre-Image Curve (ICE-PIC) method, to simplify chemical kinetics has recently been developed by Ren et al. [Z. Ren, S.B. Pope, A. Vladimirovsky, J.M. Guckenheimer, *J. Chem. Phys.* 124 (2006) 114111]. In the present work, the ICE-PIC method is first applied to the homogeneous autoignition of stoichiometric methane/air and its accuracy is shown to compare favorably to those of other methods (QSSA and RCCE). For inhomogeneous systems such as flames, spatial transport by molecular diffusion causes a small perturbation of the composition away from the attracting, low-dimensional, invariant manifold identified by the ICE-PIC method. A “close-parallel” assumption is introduced which allows this perturbation to be determined, and leads to an additional “transport coupling” term in the evolution equation for the reduced variables. For the test case of a steady, one-dimensional, laminar, methane/air flame, it is shown that the inclusion of transport coupling can reduce the dimension-reduction errors by a factor of 100. The ICE-PIC method with eight degrees of freedom (including transport coupling) exhibits comparable accuracy to a quasi-steady state assumption (QSSA) reduced mechanism with 12 degrees of freedom.

© 2006 The Combustion Institute. Published by Elsevier Inc. All rights reserved.

*Keywords:* Dimension reduction; Reduced chemistry; Low-dimensional manifold; Transport-chemistry coupling

## 1. Introduction

There is a well-recognized need to develop methodologies that radically decrease the computational burden imposed by the direct use of detailed chemical kinetics in reactive flow calculations. Of the several different types of such methodologies, three approaches that are currently

particularly fruitful (and which can be used in combination) are: the development of skeletal mechanisms from large detailed mechanisms by the elimination of inconsequential species and reactions [2]; dimension-reduction techniques [3–12]; and storage/retrieval methodologies such as ISAT [13].

In dimension-reduction methods, compositions in reactive flows are assumed to lie on (or close to) low-dimensional manifolds in the full composition space; and the chemistry is described in terms of a smaller number of reduced variables

\* Corresponding author. Fax: +1 607 255 1222.  
E-mail address: [zr26@cornell.edu](mailto:zr26@cornell.edu) (Z. Ren).

(e.g., some major species). Every dimension-reduction method constructs a low-dimensional manifold (explicitly or implicitly) in the full composition space. And each method also provides a species reconstruction technique, which, given the values of the reduced variables, identifies the corresponding full composition on the low-dimensional manifold. Many dimension reduction methods have been proposed, such as the quasi-steady state assumption (QSSA) [3,4], rate-controlled constrained equilibrium (RCCE) [5], intrinsic low-dimensional manifolds (ILDM) [6], trajectory-generated low-dimensional manifolds (TGLDM) [8], the pre-image curve method [12], and other related methodologies such as computational singular perturbation (CSP) [14].

Recently, a new dimension-reduction method—the ICE-PIC method—for simplifying combustion chemistry has been developed by Ren et al. [1]. The low-dimensional manifold employed in the ICE-PIC method is an invariant, trajectory-generated manifold. In addition, the ICE-PIC method provides a local species reconstruction technique which locally determines compositions on the low-dimensional invariant manifold. Compared to other local methods such as QSSA, RCCE and ILDM, the ICE-PIC method has the advantages of being based on an invariant manifold which is guaranteed to exist and to be continuous. It is computationally more expensive, but as discussed in [1,12] this is not a primary concern when ICE-PIC is used in conjunction with a storage/retrieval methodology such as ISAT. As demonstrated in [1], when performing species reconstruction for the one-dimensional premixed laminar hydrogen/air flame, the ICE-PIC method succeeds over the entire temperature range (including low-temperature regions). And compared with other methods such as QSSA, RCCE and ILDM, it yields the smallest maximum error.

Like most of the existing methods, the ICE-PIC method is developed for spatially homogeneous systems (absent of transport processes such as convection and diffusion), which are described by systems of ordinary differential equations (ODEs). The behavior of these reactive systems can be described by trajectories in the composition space starting from an initial condition and eventually relaxing to chemical equilibrium. However, in more realistic problems such as flames, there exist strong couplings between chemistry and transport processes. A number of studies [14–26] discuss the effects of transport in reduced descriptions of reactive flows, either in terms of a perturbation of the composition from a given manifold, or in terms of a perturbation of the manifold.

In this work, we demonstrate the application of the ICE-PIC method in both homogeneous and inhomogeneous reacting systems. In particular, we examine the accuracy of the reconstructed composition and of the rate-of-change for the

reduced composition given by ICE-PIC in comparison to other methods (QSSA and RCCE). For the inhomogeneous case, ICE-PIC is implemented in two different ways. The first is with *no transport coupling*, which amounts to the total neglect of the perturbations of compositions from the ICE manifold. In the second method, *transport coupling* is accounted for based on a “close-parallel” assumption. The results confirm that the latter method is substantially more accurate.

The paper is organized as follows. In Section 2, the ICE-PIC method is briefly described, and in Section 3, it is applied to the test case of the autoignition of a methane/air mixture. In Section 4, the issues of chemistry-reduction in the presence of transport effects are discussed, and a procedure for the ICE-PIC method to account for transport coupling is formulated. In Section 5, ICE-PIC (with and without transport coupling) is examined for the test case of a one-dimension laminar premixed flame.

## 2. The ICE-PIC method for the dimension reduction of chemical kinetics

We now provide a brief description of the invariant constrained-equilibrium edge (ICE) manifold, and of the ICE-PIC method. Full details are provided by Ren et al. [1].

To illustrate the method we consider a homogeneous, adiabatic, isobaric, closed system, of fixed enthalpy  $h$  and pressure  $p$ . Thus, the system at time  $t$  is fully described by the species specific moles (mass fractions divided by the corresponding species molecular weights),  $\mathbf{z}(t) = \{z_1, z_2, \dots, z_{n_s}\}$  of the  $n_s$  chemical species. There are  $n_e$  elements, and the specific moles of the elements are given by  $\mathbf{z}^e = \mathbf{E}^T \mathbf{z}$ , where  $\mathbf{E}$  is the  $n_s \times n_e$  element matrix such that  $E_{kj}$  is the number of atoms of element  $j$  in a molecule of species  $k$ . The system evolves according to the autonomous ordinary differential equations

$$\frac{d\mathbf{z}}{dt} = \mathbf{S}(\mathbf{z}(t)), \quad (1)$$

where  $\mathbf{S}$  denotes the net rate of change due to chemical reactions. Since elements are conserved, we have  $d\mathbf{z}^e/dt = \mathbf{E}^T \mathbf{S} = 0$ .

In the reduced description, the system is described by  $\mathbf{z}^e$  and by  $n_r$  ( $1 \leq n_r < n_s - n_e$ ) reduced composition variables  $\mathbf{r}(t) = \{r_1, r_2, \dots, r_{n_r}\}$ , which here are taken to be the specific moles of  $n_r$  user-specified “represented” species. Thus, we have  $\mathbf{r} = \mathbf{B}^T \mathbf{z}$ , where  $\mathbf{B}$  is a specified constant  $n_s \times n_r$  matrix defining the represented species. It is convenient to define the reduced composition  $\tilde{\mathbf{r}}(t)$  by

$$\tilde{\mathbf{r}} = \begin{bmatrix} \mathbf{z}^e \\ \mathbf{r} \end{bmatrix} = [\mathbf{E} \ \mathbf{B}]^T \mathbf{z} = \tilde{\mathbf{B}}^T \mathbf{z}. \quad (2)$$

Thus with  $n_{\tilde{r}} \equiv n_e + n_r$ ,  $\tilde{\mathbf{r}}$  is an  $n_{\tilde{r}} \times 1$  vector and  $\tilde{\mathbf{B}} \equiv [\mathbf{E} \ \mathbf{B}]$  is an  $n_s \times n_{\tilde{r}}$  constant matrix.

In the full composition space, realizable values of  $\mathbf{z}$  are constrained by the requirements that the specific moles be non-negative ( $z_i \geq 0$ ) and that the specific moles of elements be equal to  $\mathbf{z}^e$  (or, equivalently,  $\mathbf{E}^T \mathbf{z} = \mathbf{z}^e$ ). Correspondingly, realizable values of the reduced compositions  $\tilde{\mathbf{r}}$  are also confined to the “reduced realizable region,” denoted by  $\mathcal{C}^+$ , which is a convex polytope.

Most dimension-reduction approaches either explicitly or implicitly define (in the  $n_s$ -dimensional space of full compositions) an  $n_{\tilde{r}}$ -dimensional manifold, parameterized by the  $n_{\tilde{r}}$  reduced variables  $\tilde{\mathbf{r}}$ . Thus, there is a function  $\mathbf{z}^M(\tilde{\mathbf{r}})$  giving the full compositions on this manifold corresponding to each reduced representation  $\tilde{\mathbf{r}}$  in  $\mathcal{C}^+$ .

The ICE manifold is defined as follows. For every reduced composition  $\tilde{\mathbf{r}}$  on the boundary  $\partial\mathcal{C}^+$  of  $\mathcal{C}^+$ ,  $\mathbf{z}^{\text{ICE}}(\tilde{\mathbf{r}})$  is defined to be the constrained equilibrium composition  $\mathbf{z}^{\text{CE}}(\tilde{\mathbf{r}})$ . That is, of all compositions  $\mathbf{z}$  satisfying  $\tilde{\mathbf{B}}^T \mathbf{z} = \tilde{\mathbf{r}}$  (for the given  $\tilde{\mathbf{r}}$  in  $\partial\mathcal{C}^+$ ),  $\mathbf{z}^{\text{CE}}(\tilde{\mathbf{r}})$  is the unique composition of maximum entropy. This defines the constrained-equilibrium edge of the ICE manifold. The interior of the ICE manifold is then generated simply by following the reaction trajectories [i.e., solutions to Eq. (1)] from every point on the constrained-equilibrium edge. Thus, by construction, being composed of reaction trajectories, the ICE manifold is invariant. As is readily achieved in practice, the values of  $n_r$  and the matrix  $\mathbf{B}$  are chosen so that the ICE manifold is not folded, meaning that there is a unique manifold point  $\mathbf{z}^{\text{ICE}}$  corresponding to every value of  $\tilde{\mathbf{r}}$  in  $\mathcal{C}^+$ .

The above description implicitly yields a method by which the whole ICE manifold can be generated. However, to implement dimension-reduction strategies efficiently, it is necessary to have a local means of “species reconstruction,” that is, a method of determining  $\mathbf{z}^M(\tilde{\mathbf{r}})$  for a specified value of  $\tilde{\mathbf{r}}$ . As described in Ren et al. [1], the ICE-PIC method achieves this local species reconstruction based on the ICE manifold. Hence, this method is the first approach that locally determines compositions on a low-dimensional invariant manifold. Because it is local, the ICE-PIC method can readily be applied to high-dimensional systems. In contrast, other approaches such as the ones in [8–11], which also employ invariant manifolds, are global—they require the generation of the entire manifold. The computational implementation of such global methods soon becomes impracticable as the dimensionality of the manifold increases.

We have considered above a homogeneous system at constant pressure,  $p$ , and enthalpy,  $h$ . For clarity, we denote the method described as ICE-PIC( $p, h$ ), and Eq. (1) should be viewed as being supplemented by the equations  $dp/dt = 0$  and  $dh/dt = 0$ . As in [1], we can also consider the case

of constant pressure and temperature,  $T$ . In this case, the method is ICE-PIC( $p, T$ ); Eq. (1) is supplemented by  $dp/dt = 0$  and  $dT/dt = 0$ ; and the constrained-equilibrium composition  $\mathbf{z}^{\text{CE}}(\tilde{\mathbf{r}})$  is determined by minimizing the Gibbs function (instead of maximizing entropy).

### 3. Application to the autoignition of methane

In this section, we demonstrate the application of the ICE-PIC method in a homogeneous system without transport processes, namely, the adiabatic, isobaric autoignition of a stoichiometric methane/air mixture with an initial temperature of 1500 K and pressure of 1 atm. Quantitative comparisons are made with other methods, namely RCCE and QSSA.

With the detailed GRI1.2 [27] mechanism (which has 4 elements and 31 species), the ODEs governing isobaric, adiabatic reaction (i.e., Eq. (1),  $dp/dt = 0$  and  $dh/dt = 0$ ) are solved to yield profiles of the full composition, denoted by  $\mathbf{z}^A(t)$ . (The GRI1.2 mechanism is used to facilitate comparison with the established QSSA reduced mechanism ARM1 [28].) At different times during this autoignition process, the ICE-PIC( $p, T$ ) method is employed to perform species reconstruction, i.e., to determine the full composition  $\mathbf{z}^{\text{ICE}}$  on the corresponding ICE manifold as an estimate of  $\mathbf{z}^A$ . At each time, the thermochemical state is completely specified by pressure  $p$ , temperature  $T$  and the species specific moles  $\mathbf{z}$ ; and given the reduced representation  $\tilde{\mathbf{r}} = \tilde{\mathbf{B}}^T \mathbf{z}^A$ , the ICE-PIC( $p, T$ ) method is applied to determine  $\mathbf{z}^{\text{ICE}}(\tilde{\mathbf{r}})$ . Since the autoignition occurs at constant enthalpy, the use of ICE-PIC( $p, T$ ) (rather than ICE-PIC( $p, h$ )) provides a more stringent test of the methodology.

In the case considered (denoted as B7), there are seven represented species: CH<sub>4</sub>, O<sub>2</sub>, CO<sub>2</sub>, H<sub>2</sub>O, CO, H and O. Thus with given values of  $p$ ,  $T$  and  $\mathbf{z}^e$ , the dimension of the low-dimensional manifold is 7. For comparison, we also apply RCCE and QSSA to perform species reconstruction. With the same reduced representation as in the ICE-PIC method, the RCCE method takes the constrained-equilibrium manifold (CEM) as the low-dimensional attracting manifold and hence the reconstruction is  $\mathbf{z}^{\text{RCCE}}(\tilde{\mathbf{r}}) = \mathbf{z}^{\text{CE}}(\tilde{\mathbf{r}})$ . In ICE-PIC and RCCE, the same reduced representation  $\tilde{\mathbf{r}}$  is used, and hence these two methods can be compared directly. In QSSA, on the other hand, the reduced representation is  $\mathbf{r}$ , with no information about the elemental composition of the unrepresented species. As a consequence, the comparison with QSSA is somewhat less direct. Here we consider ARM1 [28] which has  $n_r = 16$  major species. Given that there are four elements, the dimensionality of the low-dimensional manifolds of ARM1 is 12. With the values of the major

species specific moles  $\mathbf{r} = \mathbf{B}^T \mathbf{z}^A$  being taken from  $\mathbf{z}^A$ , the minor species are reconstructed from the quasi-steady state approximation to yield  $\mathbf{z}^{\text{QSSA}}(\mathbf{r})$ .

With  $\mathbf{z}^M$  denoting the reconstructed species specific moles using one of the three methods (i.e.,  $\mathbf{z}^M$  is  $\mathbf{z}^{\text{ICE}}$ ,  $\mathbf{z}^{\text{RCCE}}$  or  $\mathbf{z}^{\text{QSSA}}$ ), we define the normalized species-reconstruction error as

$$\varepsilon_z = 2 \times |\mathbf{z}^M - \mathbf{z}^A| / (|\mathbf{z}^M| + |\mathbf{z}^A|), \quad (3)$$

where  $|\mathbf{z}|$  denotes the 2-norm. The normalized error in the rate-of-change for the reduced composition  $\mathbf{r}$  is defined as

$$\varepsilon_{\dot{\mathbf{r}}} = |\dot{\mathbf{r}}(\mathbf{z}^M) - \dot{\mathbf{r}}(\mathbf{z}^A)| / S_{\max}, \quad (4)$$

where  $\dot{\mathbf{r}} = \mathbf{B}^T \mathbf{S}$  is the rate-of-change vector for  $\mathbf{r}$ , and  $S_{\max}$  is the maximum of  $|\mathbf{S}(\mathbf{z}^A)|$  during the autoignition process.

Figure 1 shows the normalized errors in the reconstructed composition and the rate-of-change for all three methods. It is readily observed that the ICE-PIC method yields errors typically 2 or 3 orders of magnitude smaller than the corresponding RCCE method. With 7 degrees of freedom, the ICE-PIC method yields comparably accurate results with ARM1 which has 12 degree of freedom. For higher temperatures,  $T > 1800$  K, the ICE-PIC method incurs much

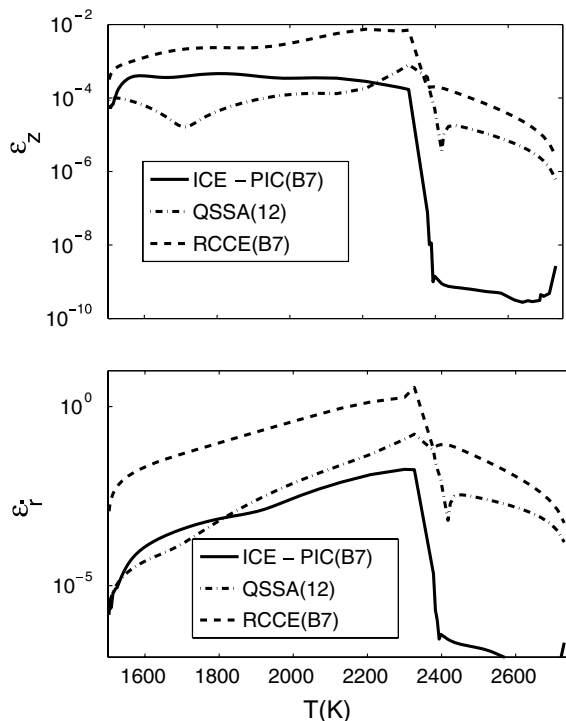


Fig. 1. Normalized species reconstruction errors Eqs. (3) and (4) as functions of temperature for the autoignition of stoichiometric  $\text{CH}_4/\text{air}$  at 1 atm. QSSA(12) denotes the ARM1 QSSA method in which there are 12 degrees of freedom; ICE-PIC and RCCE have 7 degrees of freedom.

smaller errors in the rate-of-change vector  $\dot{\mathbf{r}}$  than ARM1—two orders of magnitude smaller for  $T > 2350$  K. The maximum errors in  $\dot{\mathbf{r}}$  for ICE-PIC B7 and ARM1 during the autoignition process are 0.018 and 0.17, respectively.

#### 4. Reduced description of inhomogeneous systems via invariant manifolds

We now extend our considerations to the inhomogeneous case so that the species specific moles  $\mathbf{z}(\mathbf{x}, t)$  vary in space,  $\mathbf{x}$ , and time,  $t$ . For simplicity of exposition we continue to take the pressure and enthalpy to be constant and uniform, although the extension to variable enthalpy is straightforward.

The species conservation equation is written

$$\frac{\partial}{\partial t} \mathbf{z}(\mathbf{x}, t) = \mathbf{G}\{\mathbf{z}(\mathbf{x}, t)\} + \mathbf{S}(\mathbf{z}(\mathbf{x}, t)), \quad (5)$$

where, as previously,  $\mathbf{S}$  denotes the chemical source term, and the operator  $\mathbf{G}$  denotes convective ( $\mathbf{C}$ ) and diffusive ( $\mathbf{D}$ ) contributions,  $\mathbf{G} = \mathbf{C} + \mathbf{D}$ , where in general the convection is  $\mathbf{C}\{\mathbf{z}\} = -v_i \frac{\partial \mathbf{z}}{\partial x_i}$  with  $\mathbf{v}(\mathbf{x}, t)$  being the velocity field. In the simplest possible case (of constant density and constant and equal diffusivities,  $\Gamma$ ) the diffusion term is  $\mathbf{D} = \tilde{\mathbf{D}}$ :

$$\tilde{\mathbf{D}} \equiv \Gamma \frac{\partial^2 \mathbf{z}}{\partial x_i \partial x_i}. \quad (6)$$

With  $\mathbf{z}(\mathbf{x}, t)$  evolving according to Eq. (5), we define the corresponding reduced composition field by

$$\tilde{\mathbf{r}}(\mathbf{x}, t) = \begin{bmatrix} \mathbf{z}^e(\mathbf{x}, t) \\ \mathbf{r}(\mathbf{x}, t) \end{bmatrix} = [\mathbf{E} \ \mathbf{B}]^T \mathbf{z}(\mathbf{x}, t) = \tilde{\mathbf{B}}^T \mathbf{z}(\mathbf{x}, t), \quad (7)$$

[cf. Eq. (2)]; and hence for given  $(\mathbf{x}, t)$  there is a corresponding manifold point  $\mathbf{z}^M(\tilde{\mathbf{r}}(\mathbf{x}, t))$ . While we are primarily concerned with the ICE manifold, the development in this section applies to any invariant manifold. As depicted in Fig. 2, we can express  $\mathbf{z}(\mathbf{x}, t)$  as

$$\mathbf{z}(\mathbf{x}, t) = \mathbf{z}^M(\tilde{\mathbf{r}}(\mathbf{x}, t)) + \delta \mathbf{z}(\mathbf{x}, t), \quad (8)$$

where  $\delta \mathbf{z}(\mathbf{x}, t)$  represents the perturbation from the manifold. The full  $n_s$ -dimensional composition space is decomposed into an  $n_r$ -dimensional represented subspace (spanned by the columns of  $\tilde{\mathbf{B}}$ ) and an  $n_u$ -dimensional unrepresented subspace (orthogonal to  $\text{span}(\tilde{\mathbf{B}})$ , with  $n_u = n_s - n_r$ ). The perturbation  $\delta \mathbf{z}$  is defined to be in the unrepresented subspace, and with  $\mathbf{U}$  being a constant  $n_s \times n_u$  orthogonal matrix spanning  $\text{span}(\tilde{\mathbf{B}})^\perp$ , this can be written

$$\delta \mathbf{z}(\mathbf{x}, t) = \mathbf{U} \delta \mathbf{u}(\mathbf{x}, t), \quad (9)$$

where  $\delta \mathbf{u} = \mathbf{U}^T (\mathbf{z}(\mathbf{x}, t) - \mathbf{z}^M(\mathbf{x}, t))$ .

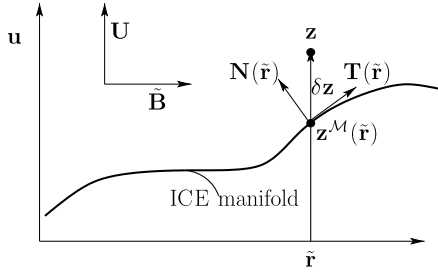


Fig. 2. A sketch in the composition space of the ICE manifold showing the representation of the general composition as  $\mathbf{z} = \mathbf{z}^M(\tilde{\mathbf{r}}) + \delta\mathbf{z}$ . The axes denote the represented variables  $\tilde{\mathbf{r}}$  (in the subspace  $\text{span}(\mathbf{B})$ ) and the unrepresented variables  $\mathbf{u}$  (in the subspace  $\text{span}(\mathbf{U}) = \text{span}(\mathbf{B})^\perp$ ). Also shown are the tangent subspace  $\text{span}(\mathbf{T}(\tilde{\mathbf{r}}))$  and the normal subspace  $\text{span}(\mathbf{N}(\tilde{\mathbf{r}}))$ .

We seek an approximate reduced description in terms of  $n_{\tilde{\mathbf{r}}}$  partial differential equations (PDEs) for  $\tilde{\mathbf{r}}(\mathbf{x}, t)$  rather than the  $n_s$  PDEs for  $\mathbf{z}(\mathbf{x}, t)$ , Eq. (5). The exact equations for  $\tilde{\mathbf{r}}(\mathbf{x}, t)$  are obtained by pre-multiplying Eq. (5) by  $\tilde{\mathbf{B}}^T$ . With the substitution  $\mathbf{z} = \mathbf{z}^M + \delta\mathbf{z}$  this yields

$$\frac{\partial \tilde{\mathbf{r}}}{\partial t} = \tilde{\mathbf{B}}^T \mathbf{G}\{\mathbf{z}^M + \delta\mathbf{z}\} + \tilde{\mathbf{B}}^T \mathbf{S}(\mathbf{z}^M + \delta\mathbf{z}). \quad (10)$$

We now consider two ways to approximate the right-hand side of Eq. (10) in terms of quantities which are known in terms of  $\tilde{\mathbf{r}}$  and  $\mathbf{z}^M$ .

#### 4.1. First approximation: neglect of perturbations

The obvious first approximation is simply to neglect the perturbations  $\delta\mathbf{z}$ , which is tantamount to assuming that  $\mathbf{z}(\mathbf{x}, t)$  lies in the manifold. From Eq. (10), this yields

$$\frac{\partial \tilde{\mathbf{r}}}{\partial t} = -v_i \frac{\partial \tilde{\mathbf{r}}}{\partial x_i} + \tilde{\mathbf{B}}^T \mathbf{D}\{\mathbf{z}^M(\tilde{\mathbf{r}})\} + \dot{\tilde{\mathbf{r}}}^M(\tilde{\mathbf{r}}), \quad (11)$$

where

$$\dot{\tilde{\mathbf{r}}}^M(\tilde{\mathbf{r}}) \equiv \tilde{\mathbf{B}}^T \mathbf{S}(\mathbf{z}^M(\tilde{\mathbf{r}})), \quad (12)$$

is the rate of change of  $\tilde{\mathbf{r}}$  on the manifold due to reactions. For the case of simplified diffusion  $\mathbf{D} = \tilde{\mathbf{D}}$ , Eq. (6), Eq. (11) becomes

$$\frac{\partial \tilde{\mathbf{r}}}{\partial t} = -v_i \frac{\partial \tilde{\mathbf{r}}}{\partial x_i} + \Gamma \frac{\partial^2 \tilde{\mathbf{r}}}{\partial x_i \partial x_i} + \dot{\tilde{\mathbf{r}}}^M(\tilde{\mathbf{r}}). \quad (13)$$

Compared to the homogeneous case, the presence of transport has no effect on reaction (according to this approximation). Hence, we refer to this approximation also as “no transport coupling.”

#### 4.2. Second approximation: close-parallel assumption

The second, improved approximation (following Tang and Pope [29]) is obtained by assuming that  $\mathbf{z}(\mathbf{x}, t)$  is close to the manifold, and that as it

evolves it moves parallel to the manifold. This “close-parallel” assumption is put into mathematical form by considering the components of Eq. (5) tangential and normal to the manifold. As depicted in Fig. 2, for given  $\tilde{\mathbf{r}}$ , we denote by  $\mathbf{T}(\tilde{\mathbf{r}})$  an  $n_s \times n_{\tilde{\mathbf{r}}}$  orthogonal matrix spanning the tangent subspace of the manifold at  $\mathbf{z}^M(\tilde{\mathbf{r}})$ , and similarly  $\mathbf{N}(\tilde{\mathbf{r}})$  is an  $n_s \times n_u$  orthogonal matrix spanning the normal subspace.

For the first term in Eq. (5), the assumption that  $\mathbf{z}$  moves parallel to the manifold amounts to the approximation  $\mathbf{N}^T \partial \mathbf{z} / \partial t \approx 0$ . For the second term, since  $\mathbf{G}$  depends on derivatives of  $\mathbf{z}(\mathbf{x}, t)$  and since by assumption  $\mathbf{z}(\mathbf{x}, t)$  is parallel to  $\mathbf{z}^M(\tilde{\mathbf{r}}(\mathbf{x}, t))$ , the indicated approximation is

$$\begin{aligned} \mathbf{N}^T \mathbf{G}\{\mathbf{z}(\mathbf{x}, t)\} &\approx \mathbf{N}^T \mathbf{G}\{\mathbf{z}^M(\tilde{\mathbf{r}}(\mathbf{x}, t))\} \\ &= \mathbf{N}^T \mathbf{D}\{\mathbf{z}^M(\tilde{\mathbf{r}}(\mathbf{x}, t))\}, \end{aligned} \quad (14)$$

where the last step follows from the fact that convection is entirely in the tangent subspace (because  $\partial \mathbf{z} / \partial x_i$  is a tangent vector). The assumption that  $\mathbf{z}$  is close to the manifold implies that  $\delta\mathbf{z}$  is small, and hence  $\mathbf{S}(\mathbf{z}) = \mathbf{S}(\mathbf{z}^M + \delta\mathbf{z})$  can be well approximated by

$$\mathbf{S}(\mathbf{z}) \approx \mathbf{S}(\mathbf{z}^M) + \mathbf{J} \delta\mathbf{z} = \mathbf{S}(\mathbf{z}^M) + \mathbf{J} \mathbf{U} \delta\mathbf{u}, \quad (15)$$

where  $\mathbf{J}$  is the Jacobian ( $J_{ik} \equiv \partial S_i / \partial z_k$ ). Now, for an invariant manifold (such as an ICE manifold),  $\mathbf{N}^T \mathbf{S}(\mathbf{z}^M)$  is zero, and hence we obtain  $\mathbf{N}^T \mathbf{S}(\mathbf{z}) = \mathbf{N}^T \mathbf{J} \mathbf{U} \delta\mathbf{u}$ . Thus, with the assumptions made, the normal component of Eq. (5) reduces to

$$0 = \mathbf{N}^T \mathbf{D}\{\mathbf{z}^M(\tilde{\mathbf{r}}(\mathbf{x}, t))\} + \mathbf{N}^T \mathbf{J} \mathbf{U} \delta\mathbf{u}. \quad (16)$$

Assuming the matrix  $\mathbf{N}^T \mathbf{J} \mathbf{U}$  to be invertible, Eq. (16) determines  $\delta\mathbf{u}$  as

$$\delta\mathbf{u} = -[\mathbf{N}^T \mathbf{J} \mathbf{U}]^{-1} \mathbf{N}^T \mathbf{D}\{\mathbf{z}^M(\tilde{\mathbf{r}}(\mathbf{x}, t))\}. \quad (17)$$

Eq. (16) represents a balance in the normal subspace between diffusion (independent of  $\delta\mathbf{u}$ ) tending to draw compositions off the manifold, and reaction providing a restoring effect, linearly proportional to  $\delta\mathbf{u}$ . For the case of simplified diffusion we obtain

$$\mathbf{N}^T \tilde{\mathbf{D}}\{\mathbf{z}^M\} = \left( \mathbf{N}^T \frac{\partial^2 \mathbf{z}^M}{\partial \tilde{r}_j \partial \tilde{r}_k} \right) \left( \Gamma \frac{\partial \tilde{r}_j}{\partial x_i} \frac{\partial \tilde{r}_k}{\partial x_i} \right), \quad (18)$$

where the first term is related to the curvature of the manifold, and the second is the dissipation rate of the reduced variables. Thus, as previously observed in [15], the combination of diffusion and manifold curvature can draw compositions off attracting manifolds.

The final evolution equation for  $\tilde{\mathbf{r}}(\mathbf{x}, t)$  is obtained from Eq. (10) again with the approximation  $\mathbf{D}\{\mathbf{z}\} = \mathbf{D}\{\mathbf{z}^M\}$  and with  $\delta\mathbf{z} = \mathbf{U} \delta\mathbf{u}$  obtained from Eq. (17):

$$\frac{\partial \tilde{\mathbf{r}}}{\partial t} = -v_i \frac{\partial \tilde{\mathbf{r}}}{\partial x_i} + \tilde{\mathbf{B}}^T \mathbf{D}\{\mathbf{z}^M(\tilde{\mathbf{r}})\} + \dot{\tilde{\mathbf{r}}}^M(\tilde{\mathbf{r}}) + \dot{\tilde{\mathbf{r}}}^D(\tilde{\mathbf{r}}), \quad (19)$$

where the final term is

$$\begin{aligned} \dot{\tilde{\mathbf{r}}}^D &= \tilde{\mathbf{B}}^T \mathbf{J} \delta \mathbf{z} \\ &= -\tilde{\mathbf{B}}^T \mathbf{J} \mathbf{U} [\mathbf{N}^T \mathbf{J} \mathbf{U}]^{-1} \mathbf{N}^T \mathbf{D}\{\mathbf{z}^M(\tilde{\mathbf{r}})\}. \end{aligned} \quad (20)$$

Notice that the evolution equation for  $\tilde{\mathbf{r}}(\mathbf{x}, t)$  (Eq. (19)) stemming from the close-parallel assumption differs from that Eq. (11) resulting from the total neglect of  $\delta \mathbf{z}$  only by the term  $\dot{\tilde{\mathbf{r}}}^D$ . This *transport coupling* term represents a perturbation to the chemical source term due to the perturbation  $\delta \mathbf{z}$  caused by diffusion.

We also observe that the two terms stemming from diffusion can be written

$$\tilde{\mathbf{B}}^T \mathbf{D}\{\mathbf{z}^M(\tilde{\mathbf{r}})\} + \dot{\tilde{\mathbf{r}}}^D(\tilde{\mathbf{r}}) = \tilde{\mathbf{B}}^T \mathbf{P} \mathbf{D}\{\mathbf{z}^M(\tilde{\mathbf{r}})\}, \quad (21)$$

where the  $n_s \times n_s$  matrix  $\mathbf{P}$

$$\mathbf{P} \equiv \mathbf{T} \mathbf{T}^T + (\mathbf{N} - \mathbf{J} \mathbf{U} [\mathbf{N}^T \mathbf{J} \mathbf{U}]^{-1} \mathbf{N}^T), \quad (22)$$

represents a particular projection onto the tangent subspace (since  $\mathbf{N}^T \mathbf{P} = 0$ ,  $\mathbf{P} \mathbf{T} = \mathbf{T}$ ). Thus the transport coupling term can also be viewed in terms of a projection of  $\mathbf{D}\{\mathbf{z}^M\}$  onto the tangent space of the manifold (cf. Maas and Pope [16] and other approaches [17–21]). The close-parallel assumption for transport coupling has been validated for a class of reaction–diffusion systems in [25]. In Ren et al. [26], examine the different approaches used to incorporate the transport coupling in the reduced description, particularly, on the connection and comparison among the current close-parallel assumption, Maas and Pope’s [16] and the ASIM approach of Singh et al. [20].

With the inclusion of transport coupling it is not guaranteed that the reconstructed composition  $\mathbf{z}^M + \delta \mathbf{z} = \mathbf{z}^M + \mathbf{U} \delta \mathbf{u}$  is realizable. We therefore investigate below a *realizability correction* in which  $\delta \mathbf{u}$  given by Eq. (17) is attenuated by a factor  $\alpha$  ( $0 \leq \alpha \leq 1$ ), which is taken to be as large as possible, subject to  $\mathbf{z}^M + \alpha \mathbf{U} \delta \mathbf{u}$  being realizable (and  $\alpha \leq 1$ ). Note that  $\alpha = 0$  corresponds to no transport coupling and guaranteed realizability.

A technical issue which may be of practical significance concerns the continuity of the projection  $\mathbf{P}$ . The ICE manifold can be considered to be composed of patches, with each facet of the boundary  $\partial \mathcal{C}^+$  generating a patch. Each patch is smooth and the manifold as a whole is continuous. Within each patch the projection  $\mathbf{P}$  therefore varies smoothly, but it may be discontinuous at patch boundaries. The projection proposed by Maas and Pope [16] is based on invariant subspaces of  $\mathbf{J}$  and hence may be discontinuous where eigenvalues cross.

Given the evolution equation Eq. (19), the reduced description is well posed given the appropriate initial and boundary conditions for  $\tilde{\mathbf{r}}$ . When using the ICE-PIC method in the reduced description of reactive flows, the initial and boundary conditions for  $\tilde{\mathbf{r}}$  can be taken directly from those corresponding to the full description. This simplicity follows from the fact that in ICE-PIC (provided the major reactants, major products and important radicals are included in the reduced compositions) the initial and boundary compositions are on the ICE manifold.

### 4.3. Implementation of diffusion

The reduced-dimension description of flames and other inhomogeneous reactive flows is given by the  $n_r$  PDEs, Eq. (19). In the numerical solution of these equations (e.g., by finite-difference methods) a storage/retrieval method such as ISAT can be used to store the  $n_r$ -vector  $\tilde{\mathbf{r}}^M$  as a function of the  $n_r$  reduced variables  $\tilde{\mathbf{r}}$  [30]. But the treatment of the diffusion term  $\tilde{\mathbf{B}}^T \mathbf{D}\{\mathbf{z}^M(\tilde{\mathbf{r}})\}$  and of the transport coupling term  $\dot{\tilde{\mathbf{r}}}^D$  is more involved. There are two obvious approaches.

The general and conceptually simple approach is to store (as functions of  $\tilde{\mathbf{r}}$ ) the manifold composition  $\mathbf{z}^M$  and the  $n_r \times n_s$  matrix  $\tilde{\mathbf{B}}^T \mathbf{P}$ . Then  $\mathbf{D}\{\mathbf{z}^M(\tilde{\mathbf{r}}(\mathbf{x}, t))\}$  can be evaluated in the full composition space, and Eq. (21) can be used to evaluate both terms arising from diffusion. The computational work and storage required by this method scale as  $n_r n_s$ .

At least with simplified diffusion, an alternative is to evaluate  $\dot{\tilde{\mathbf{r}}}^D$  entirely in the reduced space as

$$\dot{\tilde{\mathbf{r}}}^D = \left( \mathbf{V}^T \frac{\partial^2 \mathbf{z}^M}{\partial \tilde{r}_j \partial \tilde{r}_k} \right) \left( \Gamma \frac{\partial \tilde{r}_j}{\partial x_i} \frac{\partial \tilde{r}_k}{\partial x_i} \right), \quad (23)$$

where  $\mathbf{V}^T = -\tilde{\mathbf{B}}^T \mathbf{J} \mathbf{U} [\mathbf{N}^T \mathbf{J} \mathbf{U}]^{-1} \mathbf{N}^T$ , [see Eqs. (18) and (20)]. The first expression in Eq. (23) (which has  $n_r^3$  components) depends solely on  $\tilde{\mathbf{r}}$ , independent of the flow, and hence can be stored. In this case, the computational storage and work [to evaluate Eq. (23)] scale as  $n_r^3$ .

From the viewpoints of generality and ease of implementation the first method is preferable; and it may be more efficient unless  $n_r$  is much smaller than  $\sqrt{n_s}$ . But nevertheless the work and storage required  $\mathcal{O}(n_r n_s)$  is greater than that required to evaluate  $\tilde{\mathbf{r}}^M$  (i.e.,  $\mathcal{O}(n_r^2)$ ).

We note that in both approximations the conservation equation for the specific moles of elements is

$$\frac{\partial \mathbf{z}^e}{\partial t} = -v_i \frac{\partial \mathbf{z}^e}{\partial x_i} + \mathbf{E}^T \mathbf{D}\{\mathbf{z}^M(\tilde{\mathbf{r}})\}. \quad (24)$$

## 5. Application in one-dimensional premixed laminar flames

In this section, the ICE-PIC( $p, T$ ) method with and without transport coupling is investigated for a steady, isobaric, adiabatic, one-dimensional laminar flame of stoichiometric methane/air with an unburnt temperature of 298 K and pressure of 1 atm. The species conservation equation for this flame (and indeed all steady flames) is

$$0 = \mathbf{G}\{\mathbf{z}(\mathbf{x})\} + \mathbf{S}(\mathbf{z}(\mathbf{x})), \quad (25)$$

in which spatial transport balances chemical reaction.

With the detailed GRI1.2 [27] mechanism and full transport properties, the governing equations are solved to yield profiles of the full composition, denoted by  $\mathbf{z}^P$ , through the flame. The spatial transport  $\mathbf{G}\{\mathbf{z}(\mathbf{x})\}$  is conveniently extracted from the computations via Eq. (25) as  $-\mathbf{S}$ .

For the ICE-PIC method, we consider two cases, referred to as B8 and B12, which involve eight and twelve represented species. In B8, the represented species are  $\text{CH}_4$ ,  $\text{O}_2$ ,  $\text{CO}_2$ ,  $\text{H}_2\text{O}$ ,  $\text{CO}$ ,  $\text{CH}_3$ ,  $\text{H}$ ,  $\text{O}$ ; and in B12 four more species are added, namely  $\text{H}_2$ ,  $\text{OH}$ ,  $\text{CH}_2\text{O}$  and  $\text{C}_2\text{H}_4$ . Thus, with given  $p$ ,  $T$  and  $\mathbf{z}^e$ , the dimensions of the low-dimensional manifolds are 8 and 12, respectively.

At different locations across the computed flame, the temperature and the reduced composition  $\tilde{\mathbf{r}} = \mathbf{B}^T \mathbf{z}^P$  are extracted from the solution. The reconstructed composition on the ICE manifold  $\mathbf{z}^{\text{ICE}}(\tilde{\mathbf{r}})$  is then obtained using the ICE-PIC method as a first approximation of  $\mathbf{z}^P$ , i.e., with no transport coupling. The second approximation includes transport coupling and estimates  $\mathbf{z}^P$  via Eq. (17) as  $\mathbf{z}^{\text{ICE}} + \delta\mathbf{z} = \mathbf{z}^{\text{ICE}} + \mathbf{U}\delta\mathbf{u}$ , and estimates  $\tilde{\mathbf{r}}$  via Eq. (20) as  $\tilde{\mathbf{r}}^{\mathcal{M}} + \tilde{\mathbf{r}}^{\mathcal{D}}$ . For comparison, the estimates are also obtained of  $\mathbf{z}^P$  and  $\tilde{\mathbf{r}}$  given by the ARM1 QSSA mechanism, which has the same number of degrees of freedom as B12. Note, however, that this comparison may favor QSSA since it has four additional specified species.

Figure 3 shows the reconstruction errors  $\varepsilon_z$  in  $\mathbf{z}$  and  $\varepsilon_{\tilde{\mathbf{r}}}$  in  $\tilde{\mathbf{r}}$  given by QSSA and variants of ICE-PIC. The error  $\varepsilon_{\tilde{\mathbf{r}}}$  is defined the same way as in Eq. (4) except with  $\mathbf{z}^P$  replacing  $\mathbf{z}^A$  and here  $S_{\max}$  is the maximum of  $|\mathbf{S}(\mathbf{z}^P)|$  across the whole flame. The most striking observation (from Fig. 3(b)) is that the inclusion of transport coupling greatly reduces the error  $\varepsilon_{\tilde{\mathbf{r}}}$ , typically by two orders of magnitude. Over almost the entire flame the error  $\varepsilon_{\tilde{\mathbf{r}}}$  in B8 with transport coupling is less than that in QSSA and B12 (without transport coupling). With B8, the inclusion of transport coupling reduces the peak error in  $\varepsilon_{\tilde{\mathbf{r}}}$  from 0.2 to 0.002. For  $T > 700$  K, the inclusion of transport coupling in B8 reduces the reconstruction error in  $\mathbf{z}$  [ $\varepsilon_z$ , Fig. 3(a)]; and for  $T > 1500$  K the resulting errors are compara-

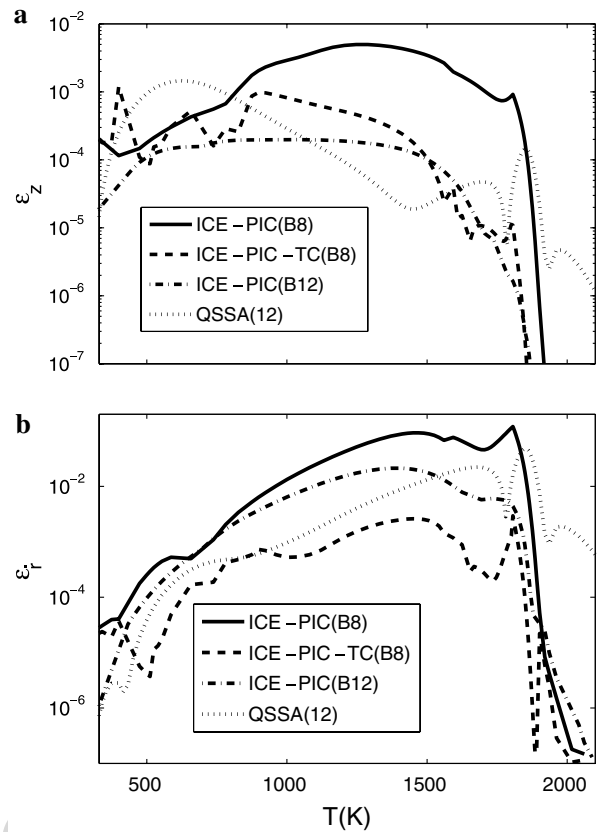


Fig. 3. Normalized reconstruction errors in (a) species  $\mathbf{z}$ , Eq. (3) (b) rate of change of reduced composition  $\tilde{\mathbf{r}}$ , Eq. (4) plotted against temperature for the one-dimensional premixed flame test case. The dashed line is ICE-PIC B8 with transport coupling; all other methods are without transport coupling.

ble to the methods with four additional degrees of freedom (B12 and QSSA).

As discussed in Section 4, the reconstructed composition is not guaranteed to be realizable when transport coupling is included. For the premixed flame test case it is found that realizability is satisfied for  $T > 750$  K. The behavior at lower temperatures is examined in Fig. 4 which shows the reconstruction errors  $\varepsilon_z$  and  $\varepsilon_{\tilde{\mathbf{r}}}$  given by B8 with and without transport coupling, and (in the former case) with and without realizability correction. As may be seen, without the realizability correction, the inclusion of transport coupling leads to relatively large errors ( $\varepsilon_z \approx 10^{-3}$  at  $T = 400$  K). With the realizability correction, the inclusion of transport coupling leads to errors  $\varepsilon_z$  which are uniformly no greater than those without transport correction, and generally orders of magnitude smaller (at higher temperatures). Interestingly, the error  $\varepsilon_{\tilde{\mathbf{r}}}$  is uniformly reduced by the inclusion of transport coupling (even when  $\mathbf{z}^{\text{ICE}} + \delta\mathbf{z}$  is non-realizable), and the realizability correction leads to an increase in  $\varepsilon_{\tilde{\mathbf{r}}}$ .

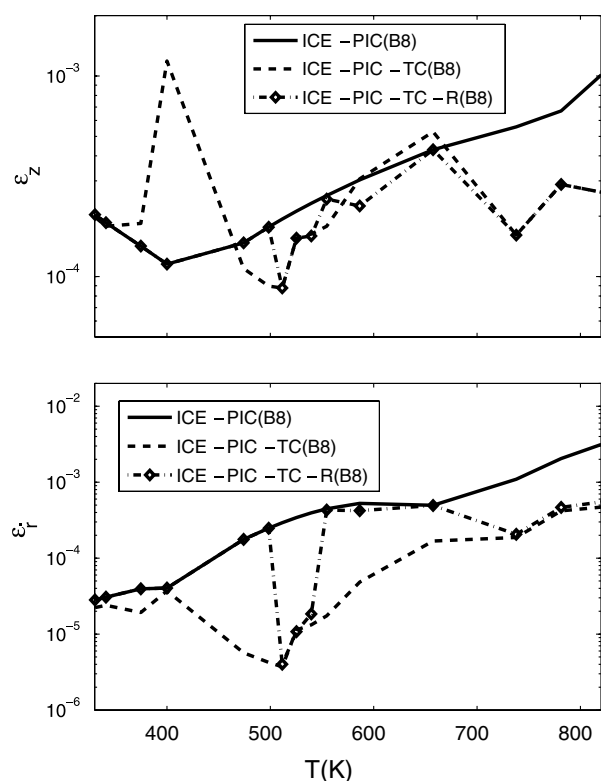


Fig. 4. Effect of transport coupling and the realizability correction on normalized reconstruction errors in the low temperature region of the premixed flame using ICE-PIC B8, solid line; no transport coupling; dashed line, transport coupling; dot-dashed line and symbols, and transport coupling with realizability correction.

## 6. Conclusion

The recently developed ICE-PIC method is investigated for two test cases involving stoichiometric methane/air: autoignition, and a one-dimension premixed laminar flame. For the autoignition test, with seven represented species, the ICE-PIC method yields comparably accurate results with ARM1 which has 12 degrees of freedom. (In the high temperature region  $T > 1800$  K, the ICE-PIC method incurs much smaller errors in the rate-of-change vector than does ARM1.)

For inhomogeneous systems, the “close-parallel” assumption is shown to lead to a transport coupling contribution  $\hat{\mathbf{r}}^D$  to the rate-of-change vector of the reduced compositions [cf. Eq. (20)]. The inclusion of transport coupling is examined in a one-dimensional premixed laminar flame of methane/air. The procedure substantially improves the accuracy in the reconstructed rate-of-change vector for the reduced composition. Hence, with transport coupling, fewer represented species are needed to describe a reactive system with given accuracy. For the one-dimensional premixed laminar flame, with 8 degrees of freedom and including transport coupling, the ICE-PIC method yields comparably

accurate results (for the rate-of-change of the reduced composition) to ARM1 which has 12 degrees of freedom. Without transport coupling, the ICE-PIC method (B12, with the same degree of freedom as ARM1) yields comparably accurate results with ARM1.

## Acknowledgment

This research is supported by the National Science Foundation through grant CTS-0426787.

## References

- [1] Z. Ren, S.B. Pope, A. Vladimirovsky, J.M. Guckenheimer, *J. Chem. Phys.* 124 (2006) 114111.
- [2] T. Lu, C.K. Law, *Proc. Combust. Inst.* 30 (2005) 1333–1341.
- [3] M. Bodenstein, S.C. Lind, *Z. Phys. Chem.* 57 (1906) 168.
- [4] M.D. Smooke (Ed.), *Reduced Kinetic Mechanisms and Asymptotic Approximations for Methane-Air Flames, Lecture Notes in Physics*, Vol. 384, Springer, Berlin, 1991.
- [5] J.C. Keck, D. Gillespie, *Combust. Flame* 17 (1971) 237–241.
- [6] U. Maas, S.B. Pope, *Combust. Flame* 88 (1992) 239–264.
- [7] J.A. van Oijen, L.P.H. de Goey, *Combust. Sci. Technol.* 161 (2000) 113–137.
- [8] S.B. Pope, U. Maas, *Simplifying Chemical Kinetics: Trajectory-Generated Low-dimensional Manifolds, FDA 93-11*, Cornell University, 1993.
- [9] M.R. Roussel, S.J. Fraser, *J. Phys. Chem.* 97 (1993) 8316–8327.
- [10] M.J. Davis, R.T. Skodje, *J. Chem. Phys.* 111 (1999) 859–874.
- [11] A.N. Gorbunov, I.V. Karlin, *Chem. Engng. Sci.* 58 (2003) 4751–4768.
- [12] Z. Ren, S.B. Pope, *Proc. Combust. Inst.* 30 (2005) 1293–1300.
- [13] S.B. Pope, *Combust. Theory Model.* 1 (1997) 41–63.
- [14] S.H. Lam, *Combust. Sci. Technol.* 89 (1993) 375–404.
- [15] S.B. Pope, *Flow, Turb. Combust.* 72 (2004) 219–243.
- [16] U. Maas, S.B. Pope, *Proc. Combust. Inst.* 24 (1992) 103–112.
- [17] S.H. Lam, Report T1953-MAE, Princeton Univ. (1992).
- [18] M. Hadjinicolaou, D.A. Goussis, *SIAM J. Sci. Comput.* 20 (1998) 781–810.
- [19] H.G. Kaper, T.J. Kaper, *Physica D* 165 (2002) 66–93.
- [20] S. Singh, J.M. Powers, S. Paolucci, *J. Chem. Phys.* 117 (2002) 1482–1496.
- [21] D.A. Goussis, M. Valorani, F. Creta, H.N. Najm, *Prog. in Comput. Fluid Dyn.* 5 (2005) 316–326.
- [22] A.N. Yannacopoulos, A.S. Tomlin, J. Brindley, J.H. Merkin, M.J. Pilling, *Physica D* 83 (1995) 421–449.
- [23] H. Bongers, J.A. van Oijen, L.P.H. de Goey, *Proc. Combust. Inst.* 29 (2002) 1371–1378.

- [24] S.S. Girimaji, C. Brau, *Theoret. Comput. Fluid Dynamics* 17 (2002) 171–188.
- [25] Z. Ren, S.B. Pope, *The Use of Slow Manifolds in Reactive Flows*, *Combust. Flame* 147 (2006) 243–261.
- [26] Z. Ren, S.B. Pope, *Transport-chemistry Coupling in the Reduced Description of Reactive Flows*, *Combust. Theory Modelling* (2006), submitted.
- [27] M. Frenklach, H. Wang, M. Goldenberg, G.P. Smith, D.M. Golden, C.T. Bowman, R.K. Hanson, W.C. Gardiner, V. Lissianski, *GRI-Mech: An Optimized Detailed Chemical Reaction Mechanism for Methane Combustion*, Gas Research Institute topical report, Gas Research Institute, Chicago, 1995.
- [28] C.J. Sung, C.K. Law, J.-Y. Chen, *Proc. Combust. Inst.* 27 (1998) 295–304.
- [29] Q. Tang, S.B. Pope, *Combust. Theory Model.* 8 (2004) 255–279.
- [30] M.A. Singer, S.B. Pope, H.N. Najm, *Combust. Theory Modelling* 10 (2) (2006) 199–217.

## Comments

*Jerry Lee, UTRC-UTC, USA.* How do you determine the dimension  $N$  of your invariant manifold *a priori*? Do you choose  $N$  according to a certain error criteria? In a reactive-diffusive system, it is likely that the slow manifold may change both in dimension and its geometry but you propose to pre-calculate a fixed manifold and then project both the chemistry source term and the diffusion term onto this fixed manifold. This can/will be a problem when the reactive diffusion system goes through phases (regions in chemistry configuration space) that correspond to different slow manifolds such as in the case of an ignition process followed by a propagating flame.

*Reply.* At the current stage, the dimensionality of the reduced description is specified manually. Then accuracy tests can be performed to determine whether or not the specified dimensionality is suitable for particular reactive flows. In the ICE-PIC approach, the ICE manifold with fixed dimensionality is employed. As long as the dimension of the manifold is high enough, the situations mentioned can be handled. Instead the method is demonstrated in the paper both for ignition and for flame propagation.

*William H. Green, MIT, USA.* You present a method for deriving the correction terms (proportional to the matrix  $H$ ) for reaction-diffusion problems. But you showed results from a reaction-diffusion problem. Does  $H$  depend on the flow field? Are there extra correction terms arising due to convection? Due to heat transfer?

*Reply.* As shown in ([25] in paper), the extra transport coupling term in Eq. (19) can be decomposed into two terms, which arise due to the effects of “dissipation-curvature” and “differential diffusion”, respectively. These extra (or correction) terms are derived from the governing PDEs (Eq. 5, which includes convection) by taking the “close-parallel” assumption. As shown in the paper, the convection process does not introduce any extra terms in the reduced description. Moreover, the shown extra terms do not depend on the flow field. The procedure proposed in this paper can be easily extended to study the effect of heat transfer (or heat loss) on the reduced description. This shows that heat transfer and heat loss introduce additional coupling terms in the reduced description of the same from as those in the specified equations.